Supporting Information for:

H₂O₂-catalyzed Defluorination of Perfluorooctanesulfonate (PFOS) by Oxidized Vanadium Carbide MXene Nanosheets

Yuemei Ye[a,§], Jessica M. Steigerwald[a], Hojeong Bang[a], Vivian Jones[b], Kaylie Dennehy[a], and Jessica R. Ray[a,*]

[a] Department of Civil & Environmental Engineering

University of Washington, Seattle, Washington 98195-2700 USA

[b]Department of Chemical Engineering, University of Washington, Seattle, Washington 98195-2700 USA

Address: 3760 E. Stevens Way, NE

Campus Box 352700

E-mail: jessray@uw.edu

Phone: (206) 221-0791

Fax: (206) 543-1543

http:/https://ray-aimslab.com/

19 pages
experimental description
9 tables
8 figures
17 references

[*]Corresponding author e-mail: jessray@uw.edu, T: 206-221-0791

Section SI. Chemicals and experimental methods

1. **Chemicals and materials**

MAX V$_2$AlC powder (300 mesh) purchased from the Forsman Company (China) was used to prepare the V(V)-C nanosheets. The Al layer was etched using hydrofluoric acid (HF, ACS grade, 48 wt%, Sigma Aldrich, MO). Vanadium pentoxide (V$_2$O$_5$, 99.95% trace metals basis, Sigma Aldrich, MO) and vanadium (III) oxide (V$_2$O$_3$, 99.99% trace metals basis, Sigma Aldrich, MO) were used as comparative vanadium-containing reaction systems. Perfluorooctanesulfonate (PFOS, 99% purity, Sigma-Aldrich, MO) and a ^{13}C-mass labeled PFAS internal standard mixture was purchased from Wellington Laboratories, LLC (Overland Park, KS). Dimethyl sulfoxide (DMSO) (anhydrous, ≥ 99.9%, Sigma Aldrich, MO) was used for the intercalation of HF-treated V$_2$C. Ethanol (≥ 99.5%, GR, Decon Laboratories. Inc., PA) was used for washing the as-prepared V(V)-C nanosheets. Tert-butyl alcohol (TBA) (99%, VWR International, LLC., PA) and sodium nitrate (NaNO$_3$, Sigma Aldrich, MO) were used to scavenge hydroxyl radicals and solvated electrons in water. Hydrogen peroxide (H$_2$O$_2$, 30%, Sigma Aldrich, MO) was used to promote reactive oxygen species and solvated electron formation in the presence of V(V)-C nanosheets. 2,2,6,6-tetramethyl-4-piperidinol (TEMP, 48 wt%, Sigma Aldrich, MO) and 5,5-dimethyl-1-pyrroline N-oxide (DMPO, Sigma Aldrich, MO) were used to capture singlet oxygen, and hydroxyl radicals and solvated electrons generated in solution during EPR measurement. FCC grade methanol, acetonitrile, water, and isopropyl alcohol were all acquired from Spectrum Chemical Manufacturing Corp. (New Brunswick, NJ) as solvents for liquid chromatography-tandem mass spectrometry (LC-MS/MS) measurements in addition to an ammonium acetate (LiChropur™, eluent additive for LC-MS/MS, Sigma Aldrich, MO) additive for PFAS quantification. Nitric acid (HNO$_3$, 69% veritas, redistilled, trace metal grade, GFS Chemicals Inc, Columbus, OH) and NaOH (beads, >97.0%, Fisher Chemical, MA) solutions were used to adjust solution pH. Catalase (from bovine liver, aqueous suspension, 10,000-40,000 units/mg protein, Sigma Aldrich, MO) was added to reaction solutions containing H$_2$O$_2$ during sampling to remove residual before ion chromatography analysis. Sodium carbonate (NaCO$_3$, 99.95-100.05%, Aldrich Chemical Company Inc., MO) and sodium bicarbonate (NaHCO$_3$, 99%, Thermo Scientific, MA) served as the eluent additives for the ion chromatography system.

2. V$_2$AlC MAX and V(V)-C nanosheet characterization

XRD samples were deposited onto XRD silicon wafer plates and air-dried prior to XRD analysis. XRD scanning was performed using a 2-theta range from 5 to 90 and a step size of 0.05 with a Cu K-α microfocus X-ray source. XPS spectra were measured using a monochromatized Al source and a spot size of 800 × 800 μm. All XPS samples were run as insulators, and a charge neutralizer was applied during the measurement. For XPS, approximately 200 μL of the V(V)-C nanosheet solution was deposited on the wafer surface for air drying prior to testing. Three spots were tested per sample and the average value of the three spots was used for atomic percentage calculations. The pass energy for the full scan survey spectra was 150 eV, and the pass energy for the high-resolution sample spectra was 50 eV. All binding energies for high-resolution spectra were referenced to C 1s C–C bonds at 285 eV which corresponds to adventitious carbon.[1]

3. Sample preparation for PFOS degradation and defluorination kinetics experiments

a. PFOS degradation analysis

A Waters 2795 Separations Module was used to load the sample, then the sample was passed through a guard column (Agilent, XDB-C18, CA) pre-filter and separated in the Agilent XDB-C18 column at a rate of 0.4 mL/min. 10 mM ammonium acetate in methanol and 10 mM ammonium acetate in water serve as the eluents to separate PFAS in the column (**Table S5b**). The separated compounds were detected in the Waters Quattro Micro API Mass Spectrometer system (Waters Corporation, Manchester, UK) detector (**Table S5a**). Additional information regarding ionization parameters, retention time, and other quantification metrics is provided in **Table S5**.

b. PFOS defluorination analysis

The **V(V)-C+H$_2$O$_2$** system sample preparation is as described: 900 µL of H$_2$O$_2$ stock solution (98 mM) was added to a solution containing 300 µL of 1 mg/mL PFOS and 4,800 µL of as-prepared V(V)-C nanosheets solution to initiate PFOS degradation in a final reaction mixture of 50 µg/L PFOS, 0.15 mg/mL V(V)-C and 14.7 mM H$_2$O$_2$. 300 µL of 1 mg/mL PFOS and 900 µL ultrapure water were added to 4800 µL of as-prepared V(V)-C nanosheets solution to obtain a mixture of 0.15 mg/mL V(V)-C and 50 µg/L PFOS for the **V(V)-C** reaction systems. As before, TBA (final concentration: 158 mM) was added to scavenge hydroxyl radicals in the solution.

A 10 mg/mL PFAS stock solution in methanol was prepared for batch studies. The 50 µg/L PFOS solution for degradation experiments was diluted from a 1 mg/L intermediate stock solution prepared in water to improve the accuracy of measured PFOS concentrations and minimize the impacts of methanol.

For **V(V)-C+H$_2$O$_2$** system samples, 20 µL of a 0.6 mg/mL catalase solution (0.0019 mg/mL final) was added after sample filtration to quench the residual H$_2$O$_2$ in the solution. In addition, the pH of the sample was adjusted to 7 before adding catalase to ensure that the added catalase would maintain high reactivity in solution.[4] A pH test strip was used to determine the solution pH during IC sample preparation. To keep the reaction volume similar across all samples, an additional 20 µL of ultrapure water was added to the **V(V)-C** system and **blank V(V)-C** system samples. All of the aforementioned samples were rotated overnight (Fisher Brand™ Multi-Purpose Tube Rotators, Fisher Scientific, MA) at 40 rpm to sufficiently decompose H$_2$O$_2$.

The **V(V)-C+H$_2$O$_2$** reaction system was centrifuged for 1 hour at 13,000 rpm, then the supernatant was removed and filtered with the 0.02 µm filters discarding the first 1 mL of filtrate to collect the remaining 5 mL of sample for IC analysis. To minimize the adsorption of F$^-$ ions to the aluminum syringe filter material, before filtering the treated sample with 0.02 µm syringe filters (aluminum base), the pH of the collected supernatant was adjusted to 9.0 which was reported to minimize F$^-$ adsorption to aluminum.[5] A Dionex IonPac AG4A-SC 4 mm guard column (Fisher Scientific, MA) connected to a Dionex IonPac AS4A-SC 4 mm analytical ion column (Fisher Scientific, MA) was used for fluoride separation at a flow rate of 1.1 mL/min carried by 1.75 mM NaHCO$_3$ and 1.8mM Na$_2$CO$_3$ eluent

2. Defluorination efficiency calculation

The PFOS defluorination efficiency at the elevated PFOS concentration was determined by subtracting the F^- concentration in **blank V(V)-C** samples (i.e., 0.15 mg/mL V(V)-C).

The defluorination efficiency (%)[6] was calculated as shown below:

Defluorination rate (%) = $\left(\dfrac{538.22 * \Delta CF^-}{C0 \times 19 * 17} \right) \times 100\%$

For the **V(V)-C+H₂O₂** system: $\Delta C_F^- = C_F^-$ (**V(V)-C +H₂O₂**) - C_F^- (**blank V(V)-C**)

For the **V(V)-C** system: $\Delta C_F^- = C_{F-}$ (**V₂C**) - C_F^- (**blank V(V)-C**)

where C_F^- (**V(V)-C +H₂O₂**) is the fluoride ion centration detected in the **V(V)-C+H₂O₂** sample, C_F^- (**V₂C**) is the fluoride ion centration detected in the **V(V)-C** sample and C_F^- (**blank V(V)-C**) is the fluoride ion centration detected in the V(V)-C only sample. More information on PFOS degradation by V_2O_3 and V_2O_5 is provided in **Section SV**.

Section SII. Syringe filter material for PFAS separation

To minimize the loss of PFOS due to filtration, we compared 0.2 μm nylon syringes of three different brands: VWR (25 mm diameter, VWR International LLC, PA), Fisher (13 mm diameter, Fisher Scientific, MA), and Pall Corporation (13 mm diameter, Pall Corporation, New York). Results of PFOS loss during filtration are summarized in **Table S1**. Even after wasting 7 mL of (50 μg/L) PFAS, the 8th mL collected filtrate showed that the nylon filter absorbed almost 100 % of PFOS from the 50 μg/L PFOS and 50 μg/L perfluorooctanoic acid (PFOA) mixture. Less PFOA loss was observed after filtering this mixture in the 8th mL collected filtrate, which agrees with an earlier report stating that nylon more easily adsorbs compounds with sulfonic acid groups.[7]

Table S1. PFOS and PFOA loss due to filtration of solutions containing both 50 μg/L PFOS and 50 μg/L PFOA in water after filtering by 0.2 μm nylon syringe filter of three different brands.

nylon filter brand	collected filter liquor	loss of PFOS (%)	loss of PFOA (%)
	1st mL	100	99.9
VWR	4th mL	100	99.8
	8th mL	99.9	87.7
	1st mL	100	100
Fisher	4th mL	100	100
	8th mL	99.9	97.2
	1st mL	100	100
Pall Corporation	4th mL	99.9	45.9
	8th mL	100	22.4

Due to the high degree of PFOS loss on nylon syringe filters, we performed a similar test examining different syringe filter materials including polyethersulfone (VWR International, LLC, PA) and cellulose acetate (VWR International, LLC, PA). The 50 μg/L PFOS only control samples were filtered in triplicate, and the averages are reported in **Table S2**. Both nylon and polyethersulfone syringe filters absorbed almost 100% of PFOS, while

cellulose acetate filters absorbed less than 15% of PFOS during sample filtration. As a result, cellulose acetate syringe filters were chosen for all experiments requiring filtration to minimize PFOS loss.

Table S2. PFOS loss due to filtration of 50 µg/L PFOS samples by different syringe filter materials: polyethersulfone, cellulose acetate and nylon. All filters were 25 mm in diameter. The first 250 µL of filtrate was discarded before collecting 1 mL of sample for LC-MS/MS analysis.

syringe filter material	loss of PFOS (%)
nylon	100
cellulose acetate	11.85
polyethersulfone	89

To determine the percentage of PFOS loss due to cellulose acetate syringe filter filtration at different initial PFOS concentrations, an additional filtration test was conducted at 2.5 and 10 µg/L initial PFOS concentrations. All samples were prepared in duplicate. The results are shown in **Table S3**.

Table S3. PFOS loss during filtration of different initial PFOS concentrations (2.5, 10 and 50 µg/L) filtered by cellulose acetate syringe filters. The initial 250 µL of the solution was discarded to rinse the filter membrane before collecting 1 mL of the filtrate for testing. 1 mL was collected for LC-MS characterization.

PFOS concentration (µg/L)	PFOS loss (%)	std. dev (%)
2.5	42.99	8.11
10	27.33	3.79
50	11.85	2.94

The data in **Table S3** shows that the PFOS loss could be as high as 42.99% by cellulose acetate filters during filtration of PFOS at concentrations of 2.5 µg/L. The percentage of PFOS loss decreased as the initial PFOS concentration increased. Due to these findings, the percent PFOS loss was accounted for during reporting of PFOS concentrations in the main text. The PFOS removal percentage was calculated by dividing the measured sample PFOS concentration by the measured PFOS concentration in the blank. Both the samples and control were filtered with 0.20 um cellulose acetate syringe filter before LC-MS/MS analysis.

Section SIII. Kinetics Model Calculations

The degradation kinetics of PFOS in the **V(V)-C+H$_2$O$_2$** and **V(V)-C** systems were evaluated with the linear pseudo-first-order and linear pseudo-second-order models. Both of these models have been used to describe reaction kinetics for the degradation of organics via advanced oxidation processes in previous works.[8] In systems where all but one reactant is present in excess, pseudo-second- and -first-order models can be used to describe the reaction which is assumed to depend only on the concentration of the limiting reactant.[9] Pseudo-second-order models describe systems with a much stronger dependence on reactant concentration (reaction rate is proportional to the square of concentration) compared to the pseudo-first-order model (reaction rate is proportional to concentration). The kinetic model equations are presented below (**equation S1** through

equation S4). For the linear pseudo-first-order model: the natural log of the PFOS concentration at time (t) was plotted as a function of time. Then the rate constant (k_1) and initial PFOS concentration after the fast adsorption step (C_0) were calculated from the slope and intercept of this graph using **equation S2**. For the linear pseudo-second-order model: the inverse of the PFOS concentration at time (t) was plotted against the reaction time, and the rate constant (k_2) and initial PFOS concentration after the fast adsorption step (C_0) was calculated using **equation S4** and the slope and intercept of this graph.

$$\frac{dC_t}{dt} = k_1 * C_t$$

equation S1

$$ln(C_t) = ln(C_0) - k_1 t$$

equation S2

$$\frac{dC_t}{dt} = k_2(C_t)^2$$

equation S3

$$\frac{1}{C_t} = k_2 t + \frac{1}{C_0}$$

equation S4

C_0 and C_t are the initial PFOS concentration and the concentration at time t in µg PFOS/L; t is time in minutes; and k_1 and k_2 are the pseudo-first-order and pseudo-second-order rate constants.

Section SIV. Effect of solvated electrons on PFOS destruction

To illustrate the effect of solvated electrons on PFOS defluorination within the **V(V)-C+H$_2$O$_2$** system, 10 mM NaNO$_3$ was added to quench solvated electron.[13] The same sample preparation for IC analysis was performed to determine the defluorination efficiency of this additional reaction system compared to previous conditions where solvated electrons were not scavenged. Specifically, four reaction systems were compared to determine the effect of solvated electrons on PFOS degradation: **blank V(V)-C** (0.15 mg/mL V(V)-C), **V(V)-C+H$_2$O$_2$** (0.15 mg/mL V(V)-C, 300.5 µg/L PFOS, and 14.7 mM H$_2$O$_2$), **NaNO$_3$-blank V(V)-C** (0.15 mg/mL V(V)-C and 10 mM NaNO$_3$), and **NaNO$_3$-V(V)-C+H$_2$O$_2$** (0.15 mg/mLV(V)-C, 10 mM NaNO$_3$, 300.5 µg/L PFOS, and 14.7 mM H$_2$O$_2$). The **blank V(V)-C** was measured as a control of the **V(V)-C+H$_2$O$_2$** sample. A higher 300.5 µg/L PFOS initial concentration was used to overcome the low IC F- detection limit (i.e., 10 µg/L). All samples were prepared in triplicate. The sample treatments and the defluorination calculation were the same as the processes described for the IC test in _Section I

Section SV. PFOS defluorination by vanadium oxides

PFOS defluorination by V(V)-C nanosheets and/or 14.7 mM H$_2$O$_2$ was compared to reaction solutions containing V$_2$O$_5$ and V$_2$O$_3$. A 3 g/L suspension of vanadium oxide (V$_2$O$_5$) and vanadium (III) oxide (V$_2$O$_3$) was prepared in ultrapure water in two separate solutions. The pH of each solution was adjusted to 3.8 to match the initial pH of the **blank V(V)-C** system. After equilibration for 1 h, the solutions were filtered with 0.20 µm cellulose acetate syringe filters. The concentrations of the V$_2$O$_3$ and V$_2$O$_5$ solutions which were mixed and reacted with 50 µg/L PFOS and 14.7 mM H$_2$O$_2$ to mimic the **V(V)-C+H$_2$O$_2$** reaction system conditions were 0.32 mg/mL (**V$_2$O$_3$+H$_2$O$_2$** system) and 1 mg/mL (**V$_2$O$_5$+H$_2$O$_2$**). In this experiment, samples were reacted for 2 h and all samples were prepared in triplicate. These reaction solutions were prepared in the same manner as the **V(V)-C+H$_2$O$_2$** reaction systems described earlier. For the **V$_2$O$_5$** and **V$_2$O$_3$** control systems, ultrapure water was added instead of the volume of H$_2$O$_2$. As before, tert-butyl alcohol (TBA) was added to scavenge hydroxyl radicals after 2 h of reaction

(i.e, when most of the PFOS degradation has occurred). Samples were prepared for LC-MS/MS and IC analysis as before. The mass:charge ratio and retention time of TBA is the same as the detected mass:charge and retention time of TFA in our sample. To correct this overlap and more accurately quantify the TFA formed in our reaction systems, a 50% v/v TBA solution calibration curve was prepared and analyzed using the LC-MS/MS method for PFAS detection. The TBA concentration was calculated from the calibration curve peak area (**Table S4** and **Figure S1**) and subtracted from the final calculated TFA concentration in the reaction samples.

Table S4. The calibration data for 50% v/v TBA in ultrapure water within the range of 8-90 µL/mL.

50% v/v TBA in solution (µL/mL)	Primary Area
8	289
15	528
30	799
60	1511
90	2762
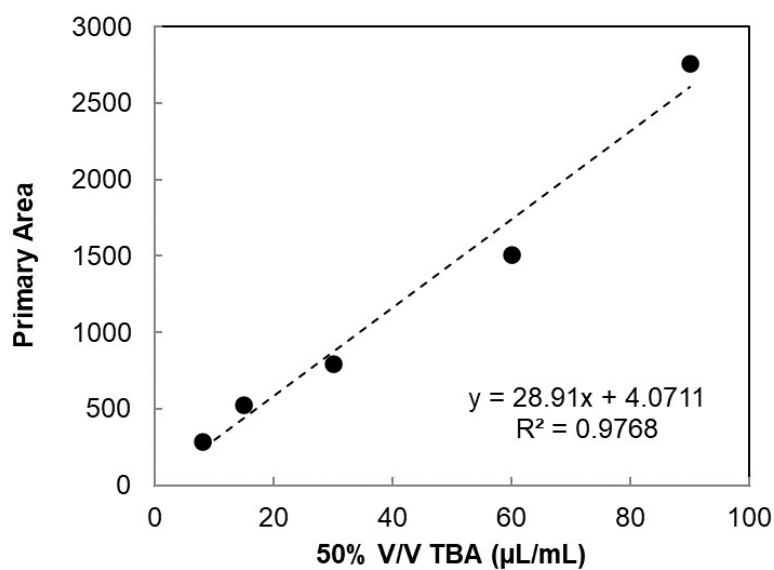
Linear calibration curve based on the data in **Table S1**, x axis is the volume of 50% v/v TBA in 1 mL of ultrapure water (µL/mL), and y axis is the primary area of TFA-69 fragment detected on the LC-MS system. The dotted line represents the linear fit of the raw data (solid circles).

Table S5. Ionization parameters, retention time (RT), and other LC-MS parameters are used to quantify perfluoroalkyl acids generated during kinetics experiments. The accompanying tables provide: **(a)** the full chemical names and structures for all compounds listed in this table; and, **(b)** the LC chromatography (e.g., eluents, gradient) associated with this quantification method. All compounds were analyzed in negative ionization mode.

PFAS	parent (m/z)	product ion (m/z)	cone (V)	collision energy (eV)	dwell (sec)	RT (min)
TFA	112.7	68.4	19	10	0.05	1.840
PFPrA	163	118.6	17	10	0.05	3.2
PFBA	213	169	11	13	0.05	5.915
mPFBA	217	172	11	13	0.05	5.930
PFPeA	263.1	68.5	17	20	0.05	7.42
PFPeA	263.1	219	17	8	0.05	7.44
mPFPeA	266.1	221	17	8	0.05	7.440
PFBS	299	79.4	14	35	0.05	7.56
PFBS	299	98.5	52	35	0.05	7.54
PFHxA	313.1	118.6	18	22	0.05	8.33
PFHxA	313.1	269.1	18	9	0.05	8.29
mPFHxA	315	270	18	13	0.05	8.29
PFPeS	348.95	79.4	54	40	0.05	8.33
PFPeS	348.95	98.5	54	35	0.05	8.315
PFHpA	363.1	168.9	17	18	0.05	8.95
PFHpA	363.1	319	18	10	0.05	8.95
PFHxS	399	79.4	54	35	0.05	8.92
PFHxS	399	98.5	54	35	0.05	8.92
mPFHxS	403	103	65	35	0.05	8.92
PFOA	413	169	18	19	0.05	9.41
PFOA	413	369.05	18	10	0.05	9.45
mPFOA	417	372	18	10	0.05	9.434
6-2 FtS	427	79.4	61	35	0.05	9.5
6-2 FtS	427	407	61	15	0.05	9.37
PFHpS	449	79.4	34	35	0.05	9.4
PFHpS	449	98.5	34	35	0.05	9.4
PFOS	498.95	79.4	53	40	0.05	9.808
PFOS	498.95	98.5	53	35	0.05	9.84
mPFOS	503.01	79.4	53	40	0.05	9.82
FTAB	569.1	223.1	25	17	0.05	9.87
FTAB	569.1	549	25	13	0.05	9.87

Table S5a.
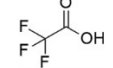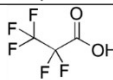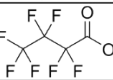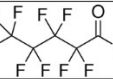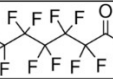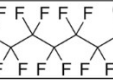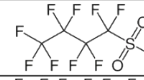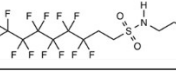
	name	acronym	structure
perfluorocarboxylic Acids (PFCAs)	trifluoroacetic acid	TFA	
	pentafluoroproprionic acid	PFPrA	
	perfluorobutanoic acid	PFBA	
	perfluoropentanoic acid	PFPeA	
	perfluorohexanoic acid	PFHxA	
	perfluoroheptanoic acid	PFHpA	
	perfluorooctanoic acid	PFOA	
perflurosulfonic Acids (PFSAs)	perfluorobutane sulfonic acid	PFBS	
	perfluoropentane sulfonic acid	PFPeS	
	perfluorohexane sulfonic acid	PFHxS	
	perfluoroheptane sulfonic acid	PFHpS	
	perfluorooctane sulfonic acid	PFOS	
polyfluoroalkyl acids	6:2 fluorotelomer sulfonate	6:2 FtS	
	8:2 fluorotelomer sulfonate	8:2 FtS	
	6:2 fluorotelomer sulfonamide alkylbetaine	6:2 FTAB	

Table S5b.

time (min)	%A (10 mM ammonium acetate)	%B (10 mM ammonium acetate in methanol)	flow rate (mL/min)
0.00	80.0	20.0	0.4
8.00	5.0	95.0	0.4
10.00	5.0	95.0	0.4
10.50	80.0	20.0	0.4
16.00	80.0	20.0	0.4

Table S6. Gradient, eluents, and flow rates used for PFOS defluorination and aqueous fluoride concentration quantification during ion chromatography analysis.

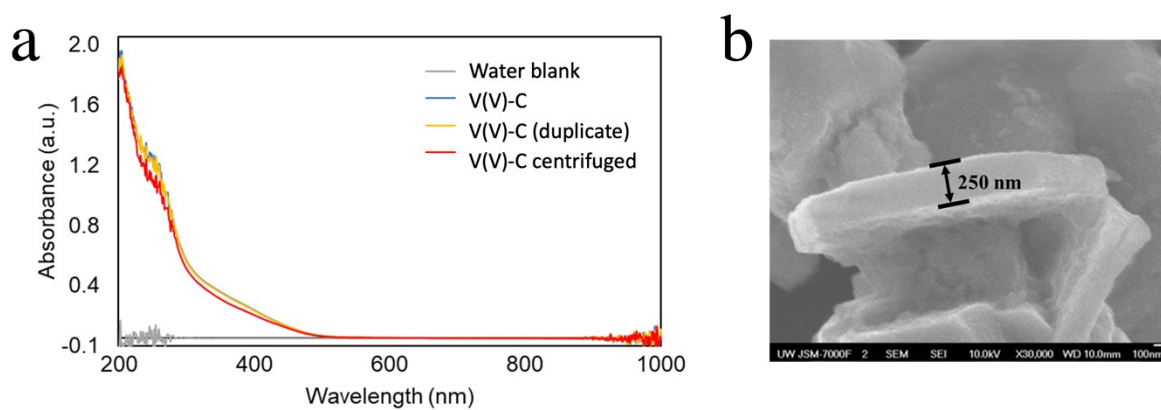| time (min)	eluent	flow rate (mL/min)
0.00	1.75 mM $NaHCO_3$ and 1.8mM Na_2CO_3	1.1
8.00	1.75 mM $NaHCO_3$ and 1.8mM Na_2CO_3	1.1

Figure S1. a. UV-Vis spectra of as-prepared V(V)-C nanosheets before and after centrifugation; b. SEM image of the single layered V(V)-C nanosheets after etching with HF acid.
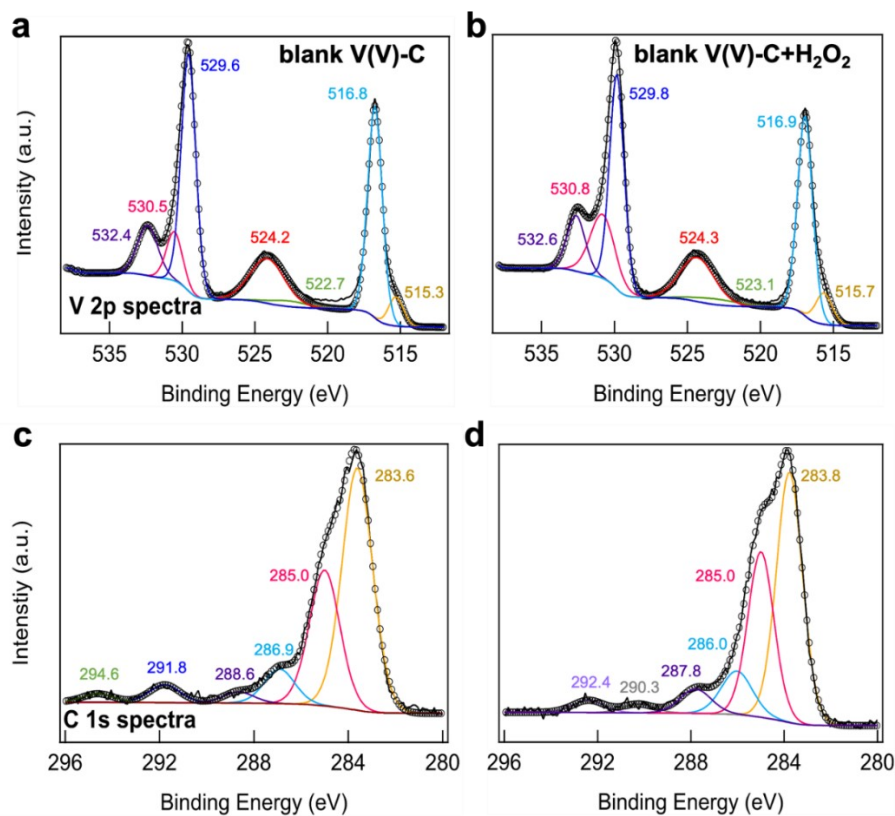
Figure S2. Fitted XPS V 2p spectra of **(a) blank V(V)-C** (i.e., 0.15 mg/mL V(V)-C) and **(b) blank V(V)-C+H₂O₂** (i.e., 0.15 mg/mL V(V)-C and overdose of H₂O₂) reaction systems. The corresponding C 1s spectra for these systems are provided in **(c)** and **(d)**, respectively.

Table S7. XPS peak identification for the reaction systems in **Figure S2**.

	peak ID	binding energy (eV)	abundance (%)	reference ID
blank V(V)-C	V 2p$_{3/2}$	515.3	4.06	515.3 eV, (V^{3+})[10]
	V 2p$_{3/2}$	516.8	29.26	516.9 eV, (V_2O_5)[11]
	V–O1s	529.6	32.8	529.8 eV, (V_2O_5)[11]
	C-C	283.6	53.9	ubiquitous C[12]
	C–O	285.0	30.1	oxidized C [11]
blank V(V)-C+H₂O₂	V 2p$_{3/2}$	515.7	4.7	515.3 eV, (V^{3+})[10]
	V 2p$_{3/2}$	516.9	27.5	516.9 eV, (V_2O_5)[11]
	V–O1s	529.8	28.1	529.8 eV, (V_2O_5)[11]
	C-C	283.8	48.0	ubiquitous C[12]
	C–O	285.0	31.7	oxidized C [11]
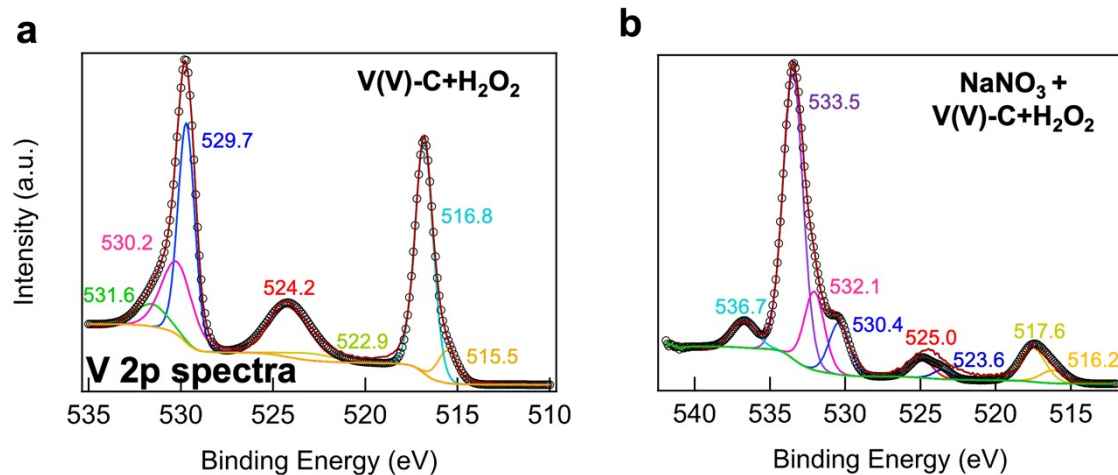
Figure S3. Fitted XPS V 2p spectra of **(a) V(V)-C+H$_2$O$_2$** and **(b) NaNO$_3$+V(V)-C+H$_2$O$_2$** reaction systems reacted for 2 hours. In both systems, the concentrations of V(V)-C, H$_2$O$_2$ and PFOS are 0.15 mg/mL, 14.7 mM and 100 µg/L, respectively. For the **NaNO$_3$+V(V)-C+H$_2$O$_2$** reaction system, 10 mM NaNO$_3$ was added before the addition of H$_2$O$_2$ and PFOS to quench solvated electrons formed in the solution.

Table S8. XPS peak identification for the reaction systems in **Figure S3**.

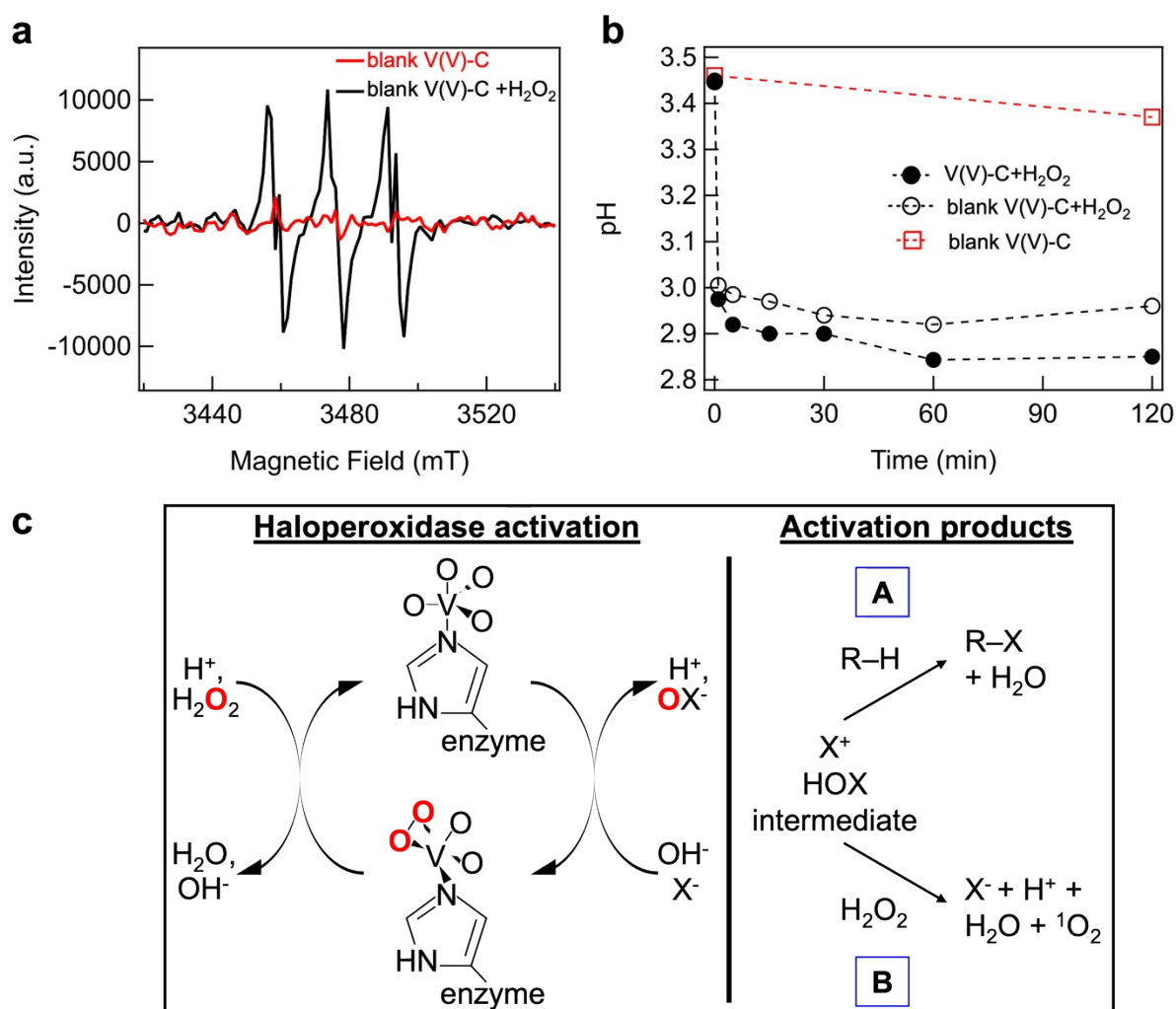|	peak ID	binding energy (eV)	abundance (%)	reference ID
	V 2p$_{3/2}$	515.5	4.68	515.3 eV, (V^{3+})[10]
V(V)-C+H$_2$O$_2$	V 2p$_{3/2}$	516.8	30.31	516.9 eV, (V$_2$O$_5$)[11]
	V–O1s	529.7	26.33	529.8 eV, (V$_2$O$_5$)[11]
	V 2p$_{3/2}$	516.2	1.4	516.2 eV, (VO$_2$)[11]
NaNO$_3$ + V(V)-C+H$_2$O$_2$	V 2p$_{3/2}$	517.6	3.6	517.7 eV, (V^{5+})[10]
	V–O1s	530.4	1.57	529.8 eV, (V$_2$O$_5$) [11]

Figure S4. (a) Electron paramagnetic resonance spectra of singlet oxygen, $^1O_2$, in ultrapure water and the **blank V(V)-C** and **V(V)-C+H$_2$O$_2$** reaction systems. The concentrations of V(V)-C and H$_2$O$_2$ are 0.15 mg/mL and 14.7 mM, respectively, and 20 mM of TEMP was added as the $^1O_2$ capture agent. **(b)** The pH resulting from the **blank V(V)-C, blank V$_2$C+H$_2$O$_2$**, and **V(V)-C+H$_2$O$_2$** reaction systems as a function of time. 50 μg/L initial PFOS concentration was added to the **V(V)-C+H$_2$O$_2$** system. **(c)** The enzymatic reaction mechanism of vanadium(V) halo peroxidase. **(a)** Schematic diagram of the reported vanadium cofactor conformational change (**left panel**) and the two corresponding reaction pathways **(A)** and **(B)** initiated upon enzyme activation (**right panel**).

The haloperoxidase enzyme found in red and brown seaweed can oxidize halides and generate $^1O_2$ in the presence of H$_2$O$_2$ as a defense mechanism against biofilm formation.[13] Haloperoxidase-like biomimetic pathway in H$_2$O$_2$-activated V(V)-C nanosheets—recently identified in the Feng et al.'s study[2]—should result in the release of H$^+$ (and decrease in pH, **Fig. S4b**), and release of fluoride when H$_2$O$_2$ exists in excess. Singlet oxygen is effective for the degradation of organic contaminants through non-radical advanced oxidation and is more selective than hydroxyl radicals.[14] Additionally, hydroxyl radicals are widely used in water treatment to oxidize and degrade contaminants;[15]
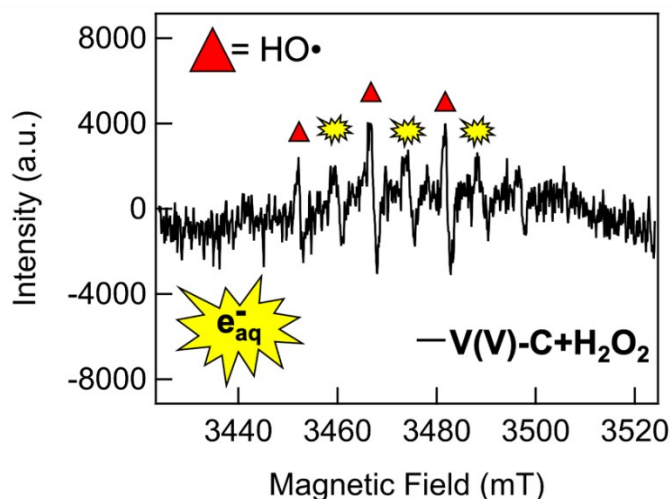
Figure S5. Electron paramagnetic resonance spectra of **blank V(V)-C+H$_2$O$_2$** reaction systems indicating formation of solvated electrons (stars above peaks). The concentrations of V(V)-C and H$_2$O$_2$ are 0.15 mg/mL and 14.7 mM, and 20 mM DMPO was added as the solvated electron capture agent. Note that the same 20 mM DMPO capture agent reveals the presence of hydroxyl radicals (i.e., triangles above peaks). Based on the collective analyses of the surface and aquatic chemistry processes occurring in the **V(V)-C** and **V(V)-C+H$_2$O$_2$** reaction systems, we propose the following reactions may occur (see below).

Biomimetic blank V(V)-C+H$_2$O$_2$ response: In the absence of PFOS, the V(V)-C nanosheet terminated F$^-$ and additional F$^-$ produced from defluorination may activate haloperoxidase enzymatic pathways. A hypofluorous acid (HOF) short half-life intermediate is formed that then rapidly degrades upon reaction with additional H$_2$O$_2$ (**Fig. S4c**, **pathway B**). Here, the H$_2$O$_2$ is serving as a reducing agent in the V(V) to V(III) two-electron transfer[16] (**Fig. 3a, b** and **Table 2**), which has been observed in other studies for reactions with V$_2$O$_5$ (i.e., vanadium(V)).[17] According to literature, in the presence of metal oxides that cannot undergo any further oxidation (i.e., V(V) on V(V)-C surfaces), H$_2$O$_2$ will catalytically decompose in two steps: (1) diffusion to the oxidized V(V)-C surface to undergo homolytic cleavage of H$_2$O$_2$ O–O bonds to form two hydroxyl radicals (**Fig. S5** and **equation S5a**); and (2) reaction with oxidized vanadium to release H$^+$ and promote electron transfer (**equation 5b**). Furthermore, because the V(V)-C nanosheet prepared in this study has a V(V) and graphite carbon heterostructure, the graphite carbon will also take part in the electron transfer reaction when H$_2$O$_2$ added as shown in **equation S6**.

$H_2O_{2(sorbed)} \rightarrow 2\ HO\cdot$ **equation S5a**

$H_2O_{2(aq)} \rightarrow 2\ H^+ + 2e^- + O_{2(g)}$ **equation S5b**
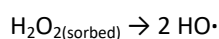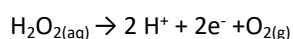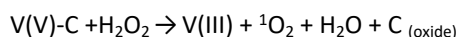
$V(V)\text{-}C + H_2O_2 \rightarrow V(III) + {}^1O_2 + H_2O + C_{(oxide)}$ **equation S6**
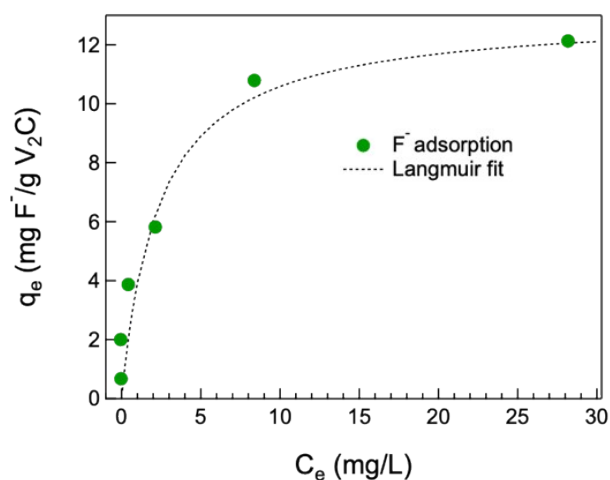
Figure S6. Langmuir adsorption isotherm fitting of F⁻ absorption onto 0.15 mg/mL V(V)-C nanosheets. A 4-h adsorption experiment was performed over a range of initial F⁻ concentrations (i.e., 0, 0.1, 0.3,1,3,10,30 mg/L sodium fluoride). Samples were mixed on a rotator at 40 rpm prior to sampling, IC sample preparation, and IC analysis to quantify adsorbed fluoride.

Table S9: The measured aqueous F⁻ concentration of a reaction system containing 4.8 mL of a V(V)-C solution in 300 µL ultrapure water after adding 900 µL H_2O_2 stock solution (98 mM) to react for 0 and 4 hours.

time (hour)	t = 0 hr	t = 4 hr
fluoride concentration (µg/L)	260 +/- 40	220 +/- 10

Table S10. Comparison of PFOS removal efficiency (50 µg/L) using different combinations of 14.7 mM H_2O_2 and 0.15 mg/mL V(V)-C nanosheets, including freshly prepared V(V)-C and V(V)-C aged for over a year in ultrapure water, after a 4-hour reaction.

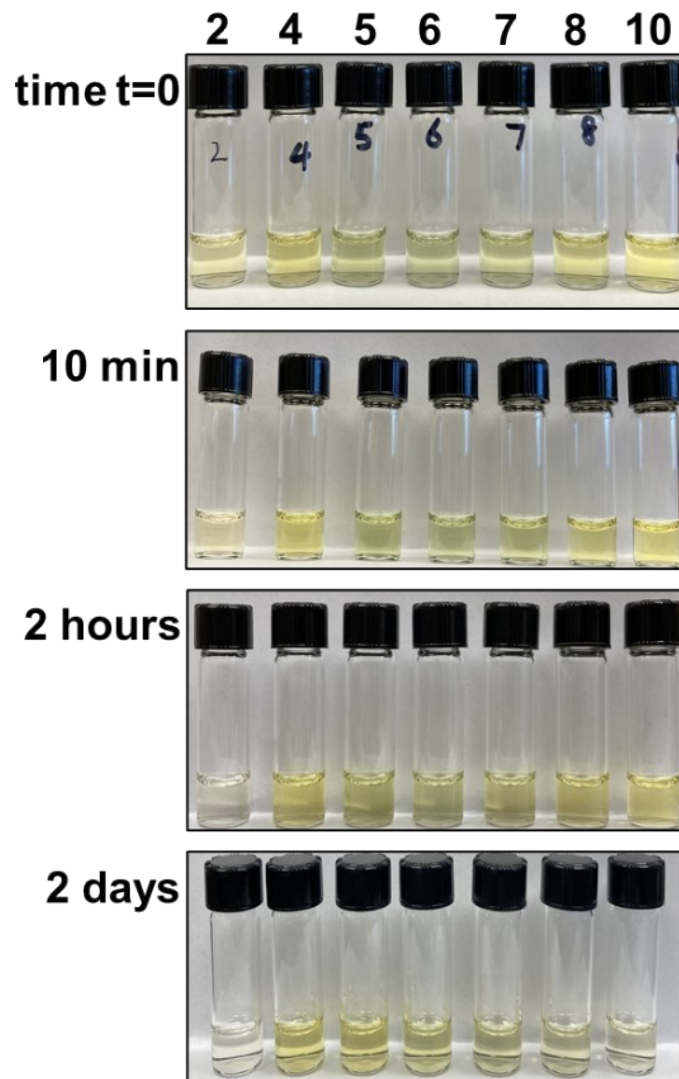| 0.15 mg/mL V(V)-C nanosheets	H_2O_2 (mM)	PFOS (µg/L)	Reacting time (hour)	PFOS removal efficiency (%)
Newly made	14.7	50	4	97.3
>1 year				96.0

Figure S7. Pictures of as-prepared V(V)-C nanosheet solutions after adjusting the pH to different values (across the top of the figure) taken at different time intervals: initially and after 10 min, 2 hours, and 2 days.
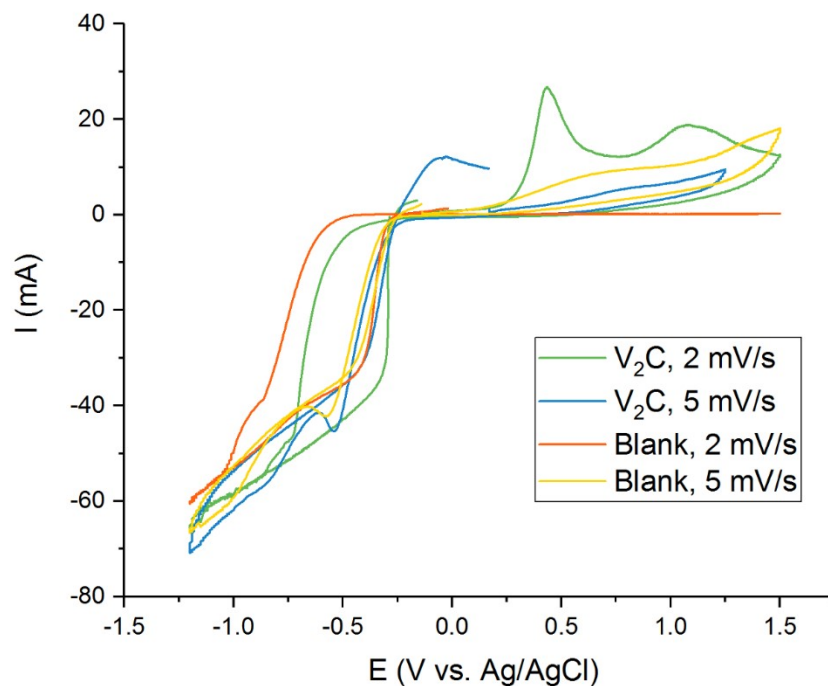
Figure S8. Cyclic voltammograms collected in 50 mM $KClO_4$ + 500 µg/L PFOS on electrodes loaded with and without V_2C MXene (i.e., **Fig. 1a2, 1b2**) powders. Scan rates of 2 and 5 mV/s were used. Working electrodes were fabricated as follows. **V_2C**: mixture of V_2C MXene powder and carbon paste painted on carbon paper and dried at room temperature. **Blank**: carbon paste painted on carbon paper and dried at room temperature.
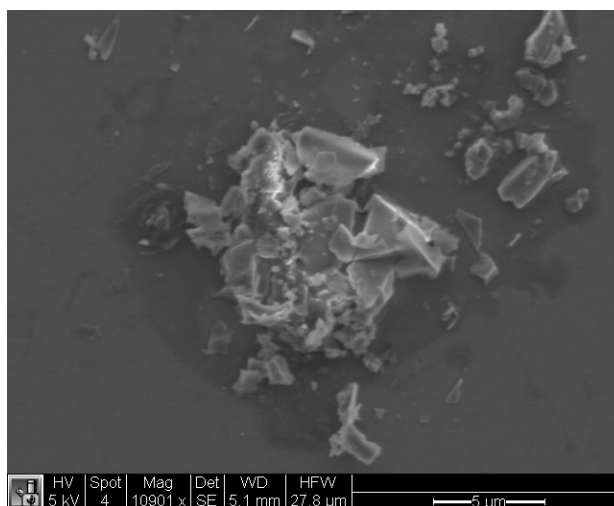

Figure S9. The SEM image of V(V)-C after reacting with H_2O_2.

References

(1) Briggs., G. B. a. D. *High Resolution XPS of Organic Polymers: The Scienta ESCA 300 Database* John Wiley & Sons, 1992.

(2) Feng, W.; Han, X.; Hu, H.; Chang, M.; Ding, L.; Xiang, H.; Chen, Y.; Li, Y. 2D vanadium carbide MXenzyme to alleviate ROS-mediated inflammatory and neurodegenerative diseases.

Nat. Commun. **2021**, *12* (1), 1-16.

(3) Jun, B.; Han, J.; Park, C. M.; Yoon, Y. Ultrasonic degradation of selected dyes using Ti$_3$C$_2$T$_x$ MXene as a sonocatalyst. *Ultraso. Sonochem.* **2020**, *64*, 104993.

(4) Chance, B. Effect of pH upon the reaction kinetics of the enzyme-substrate compounds of catalase. *J. biol. Chem.* **1952**, *194* (2), 471-481.

(5) Waghmare, S. S.; Arfin, T. Fluoride removal from water by aluminium based adsorption: A review. *J. Biol Chem. Chron.* **2015**, *1* (1), 1-11.

(6) Harrison, R. G.; Richmond, T. G. Reductive defluorination of saturated perfluorocarbons by organometallic nucleophiles. *J. Am. Chem. Soc.* **1993**, *115* (12), 5303-5304. Song, Z.; Tang, H.; Wang, N.; Zhu, L. Reductive defluorination of perfluorooctanoic acid by hydrated electrons in a sulfite-mediated UV photochemical system. *J. Hazard. Mater.* **2013**, *262*, 332-338. Tian, H.; Gao, J.; Li, H.; Boyd, S. A.; Gu, C. Complete defluorination of perfluorinated compounds by hydrated electrons generated from 3-indole-acetic-acid in organomodified montmorillonite. *Sci. Rep.* **2016**, *6*, 32949.

(7) Lath, S.; Knight, E. R.; Navarro, D. A.; Kookana, R. S.; McLaughlin, M. J. Sorption of PFOA onto different laboratory materials: Filter membranes and centrifuge tubes. *Chemosphere* **2019**, *222*, 671-678.

(8) Lyu, X.; Li, W.; Lam, P. K.; Yu, H. Insights into perfluorooctane sulfonate photodegradation in a catalyst-free aqueous solution. *Sci. Rep.* **2015**, *5* (1), 1-6. Park, H.; Vecitis, C. D.; Cheng, J.; Choi, W.; Mader, B. T.; Hoffmann, M. R. Reductive defluorination of aqueous perfluorinated alkyl surfactants: effects of ionic headgroup and chain length. *J. Phys. Chem. A* **2009**, *113* (4), 690-696. Qu, Y.; Zhang, C.; Li, F.; Chen, J.; Zhou, Q. Photo-reductive defluorination of perfluorooctanoic acid in water. *Water Res.* **2010**, *44* (9), 2939-2947.

(9) Benjamin, M. M.; Lawler, D. F. *Water quality engineering: Physical/chemical treatment processes*; John Wiley & Sons, 2013.

(10) Biesinger, M. C.; Lau, L. W.; Gerson, A. R.; Smart, R. S. C. Resolving surface chemical states in XPS analysis of first row transition metals, oxides and hydroxides: Sc, Ti, V, Cu and Zn. *Appl. Surf. Sci.* **2010**, *257* (3), 887-898.

(11) Silversmit, G.; Depla, D.; Poelman, H.; Marin, G. B.; De Gryse, R. Determination of the V2p XPS binding energies for different vanadium oxidation states (V^{5+} to V^{0+}). *J. Electron. Spectros. Relat. Phenomena* **2004**, *135* (2-3), 167-175.

(12) Naguib, M.; Halim, J.; Lu, J.; Cook, K. M.; Hultman, L.; Gogotsi, Y.; Barsoum, M. W. New two-dimensional niobium and vanadium carbides as promising materials for Li-ion batteries. *J. Am. Chem. Soc.* **2013**, *135* (43), 15966-15969.

(13) Leblanc, C.; Vilter, H.; Fournier, J.-B.; Delage, L.; Potin, P.; Rebuffet, E.; Michel, G.;

Solari, P.; Feiters, M.; Czjzek, M. Vanadium haloperoxidases: From the discovery 30 years ago to X-ray crystallographic and V K-edge absorption spectroscopic studies. *Coord. Chem. Rev.* **2015**, *301*, 134-146.

(14) Zhang, T.; Chen, Y.; Wang, Y.; Le Roux, J.; Yang, Y.; Croue, J. Efficient peroxydisulfate activation process not relying on sulfate radical generation for water pollutant degradation. *Environ. Sci. Tech.* **2014**, *48* (10), 5868-5875. Luo, R.; Li, M.; Wang, C.; Zhang, M.; Khan, M. A. N.; Sun, X.; Shen, J.; Han, W.; Wang, L.; Li, J. Singlet oxygen-dominated non-radical oxidation process for efficient degradation of bisphenol A under high salinity condition. *Water Res.* **2019**, *148*, 416-424.

(15) Hodges, B. C.; Cates, E. L.; Kim, J. Challenges and prospects of advanced oxidation water treatment processes using catalytic nanomaterials. *Nat. Nanotechnol.* **2018**, *13* (8), 642-650.

(16) Colpas, G. J.; Hamstra, B. J.; Kampf, J. W.; Pecoraro, V. L. Functional models for vanadium haloperoxidase: reactivity and mechanism of halide oxidation. *J. Am. Chem. Soc.* **1996**, *118* (14), 3469-3478.

(17) Yuan, K.; Ning, R.; Bai, M.; Hu, N.; Zhang, K.; Gu, J.; Li, Q.; Huang, Y.; Shen, C.; Xie, K. Prepotassiated V_2O_5 as the cathode material for high-voltage potassium-ion batteries. *Energy Technol.* **2020**, *8* (1), 1900796.